UC Irvine
UC Irvine Previously Published Works

Title
Diurnal and seasonal trends in the apparent density of ambient fine and coarse particles in Los Angeles

Permalink
https://escholarship.org/uc/item/7pq7k22t

Authors

Hasheminassab, Sina
Pakbin, Payam
Delfino, Ralph J
et al.

Publication Date
2014-04-01

DOI
10.1016/j.envpol.2013.12.015

Peer reviewed

Diurnal and seasonal trends in the apparent density of ambient fine and coarse particles in Los Angeles

Sina Hasheminassab[1], **Payam Pakbin**[1], **Ralph J. Delfino**[2], **James J. Schauer**[3], and **Constantinos Sioutas**[1,*]

[1]University of Southern California, Department of Civil and Environmental Engineering, 3620 South Vermont Avenue, Los Angeles, CA 90089, USA

[2]University of California, Department of Epidemiology, School of Medicine, 224 Irvine Hall, Irvine, CA 92697, USA

[3]University of Wisconsin-Madison, Environmental Chemistry and Technology Program, 660 North Park Street, Madison, WI 53706, USA

Abstract

Diurnal and seasonal variations in the apparent density of ambient fine and coarse particulate matter ($PM_{2.5}$ and CPM [$PM_{2.5-10}$], respectively) were investigated in a location near downtown Los Angeles. The apparent densities, determined by particle mass-to-volume ratios, showed strong diurnal and seasonal variations, with higher values during the warm phase (June to August 2013) compared to cold phase (November 2012 to February 2013). $PM_{2.5}$ apparent density showed minima during the morning and afternoon rush hours of the cold phase (1.20 g cm^{-3}), mainly due to the increased contribution of traffic-emitted soot particles, and highest values were found during the midday in the warm phase (2.38 g cm^{-3}). The lowest CPM apparent density was observed during the morning rush hours of the cold phase (1.41 g cm^{-3}), while highest in early afternoon during the warm phase (2.91 g cm^{-3}), most likely due to the increased wind-induced resuspension of road dust.

Keywords

particulate matter (PM); apparent density; material density; chemical composition; morphology

1. Introduction

The association between adverse health effects and exposure to ambient particulate matter (PM) has been the subject of numerous epidemiological and toxicological studies (Delfino et al., 2005; Donaldson et al., 2001; Schulz et al., 2005; Sun Q, 2005). Most of these studies have used particle mass concentration as a metric to assess the health effects of exposure to particles; however, studies have attempted to link adverse health effects with other particle characteristics such as particle size, surface area, number concentration and chemical composition (Clarke et al., 2000; Delfino et al., 2009; Li et al., 2003; Ntziachristos et al., 2007; Saldiva et al., 2002). Since the physical and chemical properties of particles are

*Corresponding author: sioutas@usc.edu, Tel: +1 213 740 6134; Fax: +1 213 744 1426.

interlinked, it is most likely that a combination of these properties may determine the overall particle toxicity. Particle density is a parameter that depends on both physical characteristics of particles (e.g. particle size, morphology and porosity) as well as their chemical composition. Moreover, density is a good predictor of the transport and depositional properties of particles in the respiratory system (Heyder, 2004). The apparent density of particles can be measured relatively easily from the ratio of particle mass to the particle volume, calculated based on the physical or equivalent volume particle diameter. The material density can also be determined by knowing the bulk chemical composition of the particles. The latter is estimated by the chemical reconstruction of PM mass, based on the relative mass fractions of the major constituents of PM.

It is often difficult to adequately characterize the chemical composition of aerosols in relatively short time intervals and the few available techniques are quite expensive. While by no means a substitute to chemical speciation measurements, near-continuous measurements of particle density are easier to conduct and have recently been reported in several urban areas around the world (DeCarlo et al., 2004; Geller et al., 2006; Khlystov et al., 2004; Malloy et al., 2009; Pitz et al., 2003; Pitz et al., 2008). To-date, however, there are only a limited number of publications in the refereed literature on the diurnal and seasonal size-resolved apparent density of ambient particles (Pitz et al., 2003; Pitz et al., 2008), particularly for the coarse PM ($PM_{2.5-10}$) size fraction.

In this study, the apparent density of ambient fine PM ($PM_{2.5}$, particles with an aerodynamic diameter smaller than 2.5 μm) and coarse PM (CPM [$PM_{2.5-10}$], particles with an aerodynamic diameter between 2.5 and 10 μm) was measured using online monitors. The volume-based size distribution of ambient particles was measured by a tandem system of a Scanning Mobility Particle Sizer (SMPS) and an Optical Particle Sizer (OPS), and the mass concentration of fine and coarse PM were measured by a Beta Attenuation Monitor (BAM) and a Continuous Coarse Particulate Matter (CCPM) monitor (Misra et al., 2001), respectively. The hourly apparent density was then calculated by the ratio of the mass to volume concentrations. The material density of $PM_{2.5}$ and CPM was also calculated based on the chemical composition data obtained from previous studies, conducted at the same sampling location. Finally, the dynamic shape factors (DSF) were estimated by the ratio of the material density to the apparent density of particles (Hand and Kreidenweis, 2002).

2. Material and methods

2.1. Sampling site and schedule

Measurements were conducted at the University of Southern California (USC) campus, about 3 km south of downtown Los Angeles. This urban site is located approximately 130 m to the east and downwind of the I-110 freeway, and is strongly affected by primary vehicular emissions, as indicated in previous studies (Geller et al., 2004; Moore et al., 2007). Measurements were conducted continuously in two separate phases; a cold phase sampling, which took place from November 2012 to February 2013, and a warm phase sampling from June to August 2013.

2.2. Equipment

The number-based size distribution of ambient particles in the range of 14 to 760 nm (equivalent mobility diameter) was measured by a Scanning Mobility Particle Sizer (SMPS, Model 3081, SN# 71207047; TSI Inc., St. Paul, MN) in conjunction with a Condensation Particle Counter (CPC, model 3020, SN# 648; TSI Inc., St. Paul, MN). The number size distribution of particles in the size range of 0.3 to 10 μm (optical diameter) was measured using an Optical Particle Sizer (OPS, model 3330, SN# 3330121205; TSI Inc., St. Paul,

MN). The OPS was factory-calibrated with Polystyrene Latex (PSL) particles, which are perfectly spherical and have a refractive index of 1.59. When particles are spherical, the size selection provided by the optical counters is very close to the actual physical (or geometric) diameter (Chen et al., 2011; Hering and McMurry, 1991; Reid et al., 1994). Moreover, the OPS response is strongly dependent on the properties of aerosols, including the refractive index and dynamic shape factor. However, there are several studies using optical particle counters calibrated by PSL particles, arguing that the refractive indices as well the shape factors of ambient aerosols are very close to those of PSL particles, particularly in urban areas (Covert et al., 1990; Ebert et al., 2004; Hänel, 1968; Kent et al., 1983; Stolzenburg et al., 1998; Strawa et al., 2006; Watson et al., 2002). Therefore further adjustment is not necessarily required for sizing the OPS, since the size errors are not significant, as will be discussed in the following section.

Volume concentration from SMPS and OPS was calculated from the number size distributions and the geometric diameters, with the assumption of spherical particles. The SMPS and OPS volume size distributions were then merged to form a composite distribution by averaging the volume concentrations within the overlap size range of the two instruments (Figure S1 a–c). Figure S1 a–c also presents the volume-based size distribution of particles, obtained from SMPS and OPS, prior to merging. It can be inferred that the agreement between the OPS and SMPS in the overlap region was overall good in both phases (less than 25% difference on an average over the overlap region), except for the first 2 channels of OPS, during the cold phase. Although both SMPS and OPS were each sampled in 5-minute intervals, hourly-averaged volume concentrations were calculated to match the hourly mass concentrations values.

The mass concentration of fine particles was measured by a Beta Attenuation Monitor (BAM 1020, SN# A4902; Met One Instruments) and the coarse PM mass concentration was measured by a co-located Continuous Coarse Particulate Matter (CCPM) monitor (Misra et al., 2001). The CCPM monitor uses a 2.5 μm cut-point virtual impactor upstream of a standard Tapered Element Oscillating Microbalance (TEOM 1400a, SN# 140AB231080006; Thermo Electron, Waltham, MA), which concentrates the CPM fraction measured by the downstream TEOM, while maintaining the $PM_{2.5}$ mass at ambient levels, providing reliable hourly CPM mass concentration (Moore et al., 2010). The mass concentration data was compared to fine and coarse PM mass concentrations reported by the South Coast Air Quality Management District (AQMD), measured at a monitoring site located approximately 5 km north of our sampling site in downtown Los Angeles, for validation, as shown in Figure S2 a–b. AQMD reports hourly $PM_{2.5}$ mass concentration measured by BAMs (identical to our method). Given the proximity of these two sites, very good agreement was observed between our $PM_{2.5}$ measurements and AQMD's data (slope=1.08 and R^2=0.75). AQMD, on the other hand, does not report CPM mass concentrations, but employs another BAM to measure PM_{10}. CPM mass concentrations can be therefore calculated by the subtraction of the reported PM_{10} and $PM_{2.5}$ mass concentrations. Due to the differences between the measurement methods as well as the more heterogeneous spatial distribution of CPM (Pakbin et al., 2010), the agreement between the values is somewhat lower, but still quite close (slope =1.06 and R^2=0.49). It should be noted that since all variables in Figures S2a and S2b have associated uncertainties, we applied Deming (or model II) linear regression solution to obtain the best estimates of the slope and intercept (York, 1966).

The black carbon (BC) content of particles was measured hourly with a Rack Mount Aethalometer (Model AE22, SN# 882; Magee Scientific, Berkeley, CA). Black carbon emission in an urban environment, such as Los Angeles, is predominantly from vehicular emissions and BC measurements in this study are used to predict daily variations of the traffic intensity.

2.3. Material and apparent densities

The material density (ρ_m) is defined as the average density of the chemical components of particles, assuming there is no internal void space in the particles (McMurry et al., 2002). The material density of a particle containing several species is expressed by (Hasan and Dzubay, 1983):

$$\rho_m^{-1} = \sum_i \frac{f_i}{\rho_i} \quad (1)$$

where ρ_m is the material density, f_i is the mass fraction for species i, and ρ_i is the material density of species i.

The apparent density (ρ_a) is defined as the ratio of particle mass to the particle volume, calculated with a diameter equal to mobility diameter (DeCarlo et al., 2004). For particles within a certain size range (d_1, d_2), apparent density is calculated by (Hu et al., 2012):

$$\rho_a = \frac{MC_{d1}^{d2}}{VC_{d1}^{d2}} = \frac{MC_{d1}^{d2}}{\frac{\pi}{6} \int_{d1}^{d2} d_p^3 \times n(d_p) d\, d_p} \quad (2)$$

where d_p is the mobility diameter, $n(d_p)$ is number concentration within a specific size range (d_1, d_2), and MC and VC are mass and volume concentrations, respectively. As mentioned earlier, the volume concentration was calculated based on the assumption of spherical particles, therefore when particles are not spherical, the apparent density may differ from the material density. Most notably, the apparent density of particles with agglomerate structures, such as diesel soot particles, is much lower than their material density. The apparent density of diesel particles with a mobility diameter of 100 nm is 0.8 g cm^{-3} and decreasing to 0.3 g cm^{-3} at 300 nm (Geller et al., 2006; Park et al., 2003) compared to pure black carbon particles having a density of 2 g cm^{-3} (Park et al., 2004).

For the apparent density calculations, the volume concentrations measured by SMPS-OPS and the mass concentrations measured by BAM and CCPM monitor were used. While the volume-based size distribution of ambient particles was calculated based on the geometric diameter (Figure S1 a–c), mass concentration measurements were based on aerodynamic diameter, since both BAM and TEOM used pre-selective impactor inlets to remove PM above a specific aerodynamic size. Therefore, to find the upper cut-points for the volume integration corresponding to fine and coarse PM mass concentrations, the mobility (or geometric) diameter was converted to an aerodynamic diameter by (Sioutas et al., 1999):

$$\sqrt{C_a}\, d_a = \sqrt{\frac{C_m \rho_p}{\chi \rho_0}}\, d_m \quad (3)$$

where d_a is the aerodynamic diameter, d_m is the mobility equivalent (or geometric) diameter, C_a is the slip correction factor for the aerodynamic diameter, C_m is the slip correction factor for the mobility equivalent diameter, χ is the dynamic shape factor, ρ_p is the bulk density of the particle, and ρ_0 is the unit density (1 g cm^{-3}). In equation (3), we assumed that $C_a = C_m = 1$ and the $\frac{\rho_p}{\chi}$ ratios (i.e., apparent densities) are equal to 1.7 and 2.1 g cm^{-3}, for PM$_{2.5}$ and CPM, respectively. The calculated upper size limits for the volume integration of PM$_{2.5}$ and CPM were found to be about 1.9 and 7.0 µm (geometric diameter), respectively. We conducted a sensitivity analysis to evaluate the effect of variations in the $\frac{\rho_p}{\chi}$ ratios on our choices in the upper size limits for the volume integrations. Ranges of variations from 1.4 to 2.0 g cm^{-3} and 1.8 to 2.3 g cm^{-3} were considered for the $\frac{\rho_p}{\chi}$ ratios (i.e., apparent densities) of

PM$_{2.5}$ and CPM, respectively. For PM$_{2.5}$ the calculated geometric diameters, corresponding to a 2.5 μm aerodynamic diameter, ranged from 1.77 to 2.11 μm, which in any case fall in the 9th channel of OPS with lower and upper boundaries of 1.73 to 2.15 μm, respectively. Also for CPM, the geometric diameters, corresponding to a 10 μm aerodynamic diameter, varied from 6.59 to 7.45 μm, which also fall in the 15th channel of OPS with lower and upper boundaries of 6.45 to 8.03 μm, respectively. The variation of upper cut-points in the aforementioned ranges results in −5 to 11% and −2 to 12% error in the calculated apparent density of PM$_{2.5}$ and CPM, respectively.

As noted earlier, the OPS response depends on the refractive index (RI) and shape factor (χ) of the sampled particles. We conducted a sensitivity analysis to evaluate the effect of variations in the RI and χ of ambient aerosols on our results. Therefore, we considered a wide range of variability from 1.51 to 1.57 for the real part of RI and 0.85 to 1.1 for the shape factor of ambient particles. These values were applied in an on-board program provided by OPS which adjusts the PSL calibration curve to a curve that better fits the aerosols of interest, by estimating the scattering intensity based on the Mie scattering theory. Table S1 shows the percent errors in the midpoint diameters compared to the base case (RI=1.59, χ =1) in all 16 channels of OPS for all extreme cases (i.e., minimum and maximum values of RI and χ). It can be seen that the size errors ranged from −19 to 15% among all channels and cases. Nonetheless, in all cases the upper size limits for the volume integrations of PM$_{2.5}$ and CPM (1.9 and 7.0 μm geometric diameters, respectively) fell into the 9th and 15th channels of OPS, respectively, consistent with our initial choices, demonstrating that the choice of our cut-point in both size fractions was reasonable. Table S2 presents the percent volume concentration errors compared to the base case, in all 16 channels of the OPS. On average across all channels, the volume concentration errors varied from −30 to 21 % among all extreme cases. The largest errors were found in channels 6 to 8, which usually contain the lowest volume concentrations among all size channels, as shown in Figure S1 a–c. Moreover, given that these channels explain a very small portion of PM$_{2.5}$ volume concentration (altogether about 12 %), their overall influence on the PM$_{2.5}$ volume and density is expected to be low. In addition, the volume concentrations of CPM, which are entirely obtained from the OPS (channels 10 to 15), varied from −27 to 17% of the base case, among all extreme cases.

2.4. Dynamic shape factor (DSF)

Dynamic shape factor (DSF), χ, is a parameter which accounts for the irregularity of particles and is defined as the ratio of the actual resistance force on a non-spherical particle to the resistance force on a spherical particle which has the same volume and velocity as the particle of interest (Hinds, 1999). According to the definition by Hand and Kreidenweis (2002), DSF can be calculated as the ratio of the particle material density to its apparent density:

$$\chi = \frac{\rho_m}{\rho_a} \quad (4)$$

The DSF is equal to one for spheres, while irregular particles have DSFs greater than one (DeCarlo et al., 2004).

2.5. Meteorology

Meteorological conditions are important factors in the interpretation of the levels and variations of particle density. Diurnal trends of selected meteorological parameters including temperature, relative humidity, wind speed and precipitation over both phases are shown in Figure 1a–d. On average, the temperature was 7 °C higher during the warm phase compared

to the cold phase. However, similar diurnal trends were observed during both phases, with minima in early morning, coinciding with the morning rush hours, and a peak during the mid-day. Relative humidity displayed a reverse trend compared to temperature, with the lowest levels in the middle of the day and highest during the nighttime. Wind speed was generally stronger during the warmer season and the maximum levels were observed during the afternoon in both phases. As can be seen in Figure 1d, precipitation was significantly higher during the cold phase, while almost zero during the warm phase. In the cold phase, the sum of precipitation after midnight and early morning was considerably higher compared to the rest of the day. It is noteworthy that from 20:00 until morning rush hours, all of meteorological parameters are almost stable, creating stagnant conditions during nighttime, especially in cooler seasons.

3. Results and Discussion

3.1. Diurnal trends in the mass and volume concentrations of $PM_{2.5}$ and CPM

The diurnal profiles of mass and volume concentrations during both phases for fine and coarse PM are shown in Figure 2a–b. A notable increase in the mass and volume concentrations of $PM_{2.5}$ is evident during the morning rush hours across seasons. Compared to the cold phase, the nighttime $PM_{2.5}$ volume concentration levels decreased in the warm phase, while its levels increased in the middle of the day. The $PM_{2.5}$ mass concentration, on the other hand, slightly increased during the warm phase, particularly during the mid-day, resulting in an overall increase in the $PM_{2.5}$ apparent density values.

Although the CPM mass and volume concentration levels were almost comparable during both phases, their diurnal variations displayed distinct patterns in each phase. During the cooler phase, after the morning commute, mass and volume concentrations of CPM rapidly decay to levels as low as 11.4 $\mu g\ m^{-3}$ and 5.9 $\mu m^3\ cm^{-3}$, respectively. These concentrations start increasing again in the early afternoon and peak around midnight. Cheung et al. (2011b) reported similar observations for CPM with elevated levels of mass concentration during the overnight period (7:00 p.m. to 7:00 a.m.) in winter, at the same sampling location. Resuspension of local road dust induced by a higher speed of traffic and heavy-duty vehicles in the very close (~100 m) proximity and upstream of our site I-110 freeway, at night, coupled with a lower mixing height during the winter might be responsible for the increase in the PM mass and volume concentrations. During the warm phase, the highest levels of CPM mass concentrations were observed in the early afternoon, when the wind speed was highest. During the same period, however, the volume concentration did not show any noticeable peaks, suggesting that the coarse particles at this time of the day were denser and had more compact structures. Similar trends and levels for the $PM_{2.5}$ and CPM mass concentrations have been previously reported by Moore et al. (2010) at the same sampling site.

3.2. Daily variation of $PM_{2.5}$ and CPM apparent density

Variation of daily-averaged apparent density of $PM_{2.5}$ and CPM in both phases is shown within box plots for each month in Figure 3. $PM_{2.5}$ apparent density significantly increased from levels around 1.4 g cm^{-3} in the cooler phase to about 2.2 g cm^{-3} in the warmer phase, while this increase in CPM was less pronounced. Given the limited atmospheric dilution of primary emissions during the cold seasons, lower values of the $PM_{2.5}$ apparent density in winter is most likely attributed to the increased concentration of agglomerate soot particles, as shown in Figure 4, with an apparent density below 1 g cm^{-3} (Pitz et al., 2003). Moreover, previous studies in this area have shown that the contribution of organic carbon (OC) from primary sources to both fine and CPM size ranges significantly increases during the winter (Saffari et al., 2013; Sardar et al., 2005). Elevated levels of OC, whose bulk density is lower

than inorganic ions, may also be responsible for the lower apparent densities in both size fractions during the cold phase (bulk densities for ammonium sulfate, ammonium nitrate, and organic aerosols are 1.77, 1.73, and 1.2 g cm^{-3}, respectively (Pitz et al., 2008; Turpin and Lim, 2001)). The elevation in the values of PM$_{2.5}$ apparent densities during the warm phase is most likely due to the enhanced production of secondary aerosols by gas and aqueous phase reactions (Blando and Turpin, 2000; Fine et al., 2004) and their condensation onto the primary emitted particles. Increased contribution of metals and trace elements, which are the key ingredients of resuspended road dust (Hu et al., 2008; Sardar et al., 2005), is responsible for the increase in the CPM apparent density during the summer. Few studies, by employing different methods, have investigated the size-segregated apparent density of ambient particles in different locations around the world. Pitz et al. (2008) reported an average of 1.68 and 1.60 g cm^{-3} for the PM$_{2.5}$ apparent density during the summer and winter, respectively, in the German city of Augsburg. Hu et al. (2012) conducted a study in Beijing for five days in January 2007 and reported an average apparent density of 1.6±0.4 g cm^{-3} for PM$_{1.8}$ and 1.9±0.6 g cm^{-3} for PM$_{1.8-10}$. At the same sampling location of this study, Geller et al. (2006) showed that during the fall season the apparent density of ambient PM in the size range of 50–414 nm (mobility diameter) varies from 0.73 to 1.14 g cm^{-3}. These values confirm that the apparent density of ambient PM varies by location with different sources of pollutants and meteorology. Figure 3 also illustrates that the apparent densities of PM$_{2.5}$ and CPM have a wide range of variation in each season, indicating that these values are affected by several factors including meteorological conditions, source emission strength, atmospheric mixing and dilution by vertical convection, all of which affect the PM chemical composition.

The spearman rank order correlation was applied to the hourly data points to determine the relationships between the apparent densities and selected parameters including black carbon mass content of PM$_{2.5}$ (BC/PM$_{2.5}$), temperature, and relative humidity, as shown in Table 1. Measured p-value in each pair of variables was less than 0.05, indicating that the relationship between each two variables was statistically significant. During the cold phase, weak correlations were found between the apparent density of both size ranges and temperature, while these values significantly increased during the warm phase. The production of secondary aerosols, with relatively higher bulk densities, increases in higher temperatures, leading to an increase in the overall apparent density of ambient PM (Kostenidou et al., 2007). In contrast, relative humidity showed a moderately negative correlation with the CPM apparent density and very low correlation with PM$_{2.5}$ apparent density during both phases. Lower relative humidity facilitates the wind-induced resuspension of larger particles comprising a higher fraction of mineral and road dust elements (Moore et al., 2010), having material densities greater than 2 g cm^{-3} (Hand and Kreidenweis, 2002; Hussein et al., 2008), resulting in an elevation in the apparent density of coarse particles. Negative correlations were observed between PM$_{2.5}$ apparent density and BC/PM$_{2.5}$. This negative correlation was much stronger during the colder phase, when BC contribution to PM$_{2.5}$ was considerably higher, as shown in Figure 4. Figure 5 shows, however, that the relationship between the hourly PM$_{2.5}$ apparent density and BC/PM$_{2.5}$ is not linear, but actually inverse. These negative correlations indicate that the apparent density of fine particles significantly decreases whenever the contribution of fresh soot particles to total mass increases, particularly in the cold phase and during the morning and afternoon rush hours.

3.3. Diurnal variation of PM$_{2.5}$ and CPM apparent density

Figure 6a–b shows the diurnal trends of PM$_{2.5}$ and CPM apparent densities in both cold and warm phases. Pronounced variations in the apparent densities reveal that particles' shape and chemical composition considerably change during the day. As discussed above and also

shown in Figure 6a, $PM_{2.5}$ apparent density levels significantly increased during the warm phase, which was accompanied by a remarkable decrease in the contribution of black carbon to $PM_{2.5}$ (Figure 4). During the cold phase, when the mixing height is lower, in the morning rush hours BC makes up nearly 14% of total $PM_{2.5}$ mass concentration (Figure 4); at the same time $PM_{2.5}$ apparent density reaches a minimum of 1.21 ± 0.07 g cm^{-3}. A similar drop in the fine PM apparent density is also observed during the warm phase in the morning rush hours. Pitz et al. (2003) determined an apparent density of 1.1 g cm^{-3} for $PM_{2.5}$ during the wintertime morning rush hour traffic in Erfurt, Germany. Another study conducted by Pitz et al. (2008) in Augsburg, an urban area in southern Germany, reported a $PM_{2.5}$ apparent density of 1.5 g cm^{-3} for the same time period of the day in winter. Decreased values in the $PM_{2.5}$ apparent density during the morning rush hours, especially in the cold phase, are mainly attributed to the enhanced contribution of fresh agglomerate soot particles, emitted from vehicular sources, when the atmospheric dispersion is limited and more stable conditions prevail. As the day progresses, $PM_{2.5}$ apparent density rises up to 1.57 ± 0.09 and 2.38 ± 0.07 g cm^{-3} in the cold and warm phases, respectively. This increase in the middle of the day is likely due to the enhanced photochemical activity and increased production of secondary aerosols (Turpin et al., 1991) which condense on pre-existing particles, filling out their void spaces, leading to an increase in their apparent densities (Nakao et al., 2011). Moreover, atmospheric aging significantly alters the hygroscopicity of the soot particles, which are initially hydrophobic. Several studies showed that aged soot particles are coated by sulfate and organics and become hydrophilic so that they can even act as cloud condensation nuclei (CCN) (Ghazi and Olfert, 2013; Khalizov et al., 2013; Schwarz et al., 2008; Shiraiwa et al., 2007). Throughout this atmospheric processing and uptake of water, the morphology of these particles is transformed to a more compact form, with a dynamic shape factor close to one; thus, the apparent density of these particles might approach their material density of about 2 g cm^{-3} (Hand and Kreidenweis, 2002; Khalizov et al., 2013; Pagels et al., 2009). An additional possible mechanism which might affect the $PM_{2.5}$ apparent density, particularly in the middle of the day during the warm phase, is the increased contribution of wind-induced road dust to the overall PM mass, given that these sources are enriched in trace elements and metals, with significantly higher material density compared to OC. Although the majority of these particles are in the coarse PM mode, it is likely that a fraction also partitions in the 1–2.5 μm range as shown by Geller et al. (2004) and Majestic et al. (2008). This hypothesis is further supported by the higher volume concentration in the lower "tail" of the super-micron PM range, extending to the upper range of $PM_{2.5}$, as shown in Figure S1 a. The second minimum in the $PM_{2.5}$ apparent density, during the colder phase, occurs in the evening rush hours at around 7:00 p.m., when the levels drop to 1.19 ± 0.05 g cm^{-3}.

Similar to $PM_{2.5}$, a drop in the CPM apparent density is observed during the early morning rush hours, with the lowest values of 1.41 ± 0.08 and 1.77 ± 0.04 g cm^{-3} during the cold and warm phases, respectively. Cheung et al. (2011b) investigated the diurnal variations in the chemical composition of coarse PM during the summer and winter at the same sampling location. They reported lower contribution of minerals and trace elements to overall CPM mass during the morning period (7:00 a.m. to 11:00 a.m.) in both seasons. Mineral dust is comprised primarily of elements such as Al, Fe, Ca (Pakbin et al., 2011) with relatively higher bulk densities (2.3–2.5 g cm^{-3} (Chou et al., 2011; Kaaden et al., 2009)) compared to other main CPM components such as sodium nitrate and organic matter (Cheung et al., 2011b). Decreased contribution of minerals and trace elements, with densities that are generally higher than other species in this size range, results in a reduction in the apparent density of CPM during the morning period. Following the morning rush hours, during the cold phase, CPM apparent density starts increasing, reaching 1.93 ± 0.10 g cm^{-3} at around 11:00 a.m. and remains high until midnight, even though the wind speed calms down in the afternoon (Figure S 3a). This is likely due to the increased contribution of mineral dust and

trace elements to total CPM during the nighttime in the winter, as documented by Cheung et al. (2011b) and discussed earlier. During the warm phase, the diurnal pattern of the CPM apparent density follows exactly that of wind speed (Figure S 3b), with minimum levels during the overnight and maximum values in early afternoon. The sharp increase in the CPM apparent density after morning rush hours is attributed to the stronger wind speeds coupled with lower relative humidity in the middle of the day, which substantially enhances the resuspension of road dust, containing higher portions of minerals and trace elements. Diurnal profiles of CPM apparent density during both phases are consistent with the diurnal variation of crustal material and trace elements reported by Cheung et al. (2011b).

3.4. Material (bulk) density and dynamic shape factor (DSF)

Material density of coarse and fine PM was calculated based on the chemical composition of size-segregated particles reported by previous studies, conducted at the same sampling location in the past 3–7 years. The use of chemical PM speciation data from earlier, though fairly recent, studies, conducted in the same location, is one of our limitations in this study. Nonetheless, we do not believe that the relative contributions of different chemical groups to the overall PM mass have changed substantially in central Los Angeles over the past few years, as evidenced by the consistent bulk density values calculated based on different sampling campaigns conducted at USC and in downtown Los Angeles (Cheung et al., 2011a; Cheung et al., 2011b; Hu et al., 2008; Ostro et al., 2009; Sardar et al., 2005; Wang et al., 2013). As presented in Table S3, the difference in the calculated material densities, for both size fractions, are quite small among the various studies and datasets. For $PM_{2.5}$, our calculations are based on the data reported by Sardar et al. (2005), since they are more comprehensive and cover an entire 12 month period as opposed to the rest of the studies that are more episodic in nature and cover few weeks/months. CPM chemical composition data were obtained from two separate studies by Cheung et al. (2011a; 2011b), since these are the only studies of this nature at that site. These studies were conducted in the 2008–2010 period, which is quite recent with respect to our current measurements, and we find it rather unlikely that the relative CPM chemical composition has changed drastically (i.e., to the point of affecting our calculations) in the interim period.

To use equation (1), chemical species were grouped into inorganic ions (nitrate, sulfate, and ammonium), other ions (sodium, potassium, calcium, and chlorine), elemental carbon (EC), organic matter (OM=OC × 1.6) and minerals (total mass concentrations subtracted by the sum of inorganic ions, other ions, EC, and OM) (Hu et al., 2012); the material density of these species were assumed to be 1.75, 2.0, 2.0, 1.2, and 2.8 g cm^{-3}, respectively, based on the recommendations by Hussen et. al (2008), Pitz et al. (2008), and Sioutas et al. (2000). As presented in Table 2, CPM has greater material density compared to $PM_{2.5}$ and levels are higher in summer compared to winter, in both size fractions. On average, CPM material density varies from 2.06 g cm^{-3} in winter to 2.36 g cm^{-3} in summer, mainly due to the increased contribution of crustal materials and trace elements to the CPM size fraction during the warmer seasons in Los Angeles. Similarly, $PM_{2.5}$ material density increases from 1.41 g cm^{-3} in winter to 1.71 g cm^{-3} in summer. The dynamic shape factors were estimated for each size fraction from the calculated material and apparent densities, using equation (4). As shown in Table 2, DSF values were overall close to 1, except for $PM_{2.5}$ during the warm phase for which DSF values were lower than (but still close to-) 1 (0.79±0.15). Moreover, the levels were generally higher in the coarse size fraction, during both phases of the study. Evidence from previous studies suggests that the DSF generally increases with increasing particle diameter, as the larger particles have more irregular shapes than the smaller ones (Kaaden et al., 2009; Reid et al., 2003). Lastly, a shape factor below one was obtained for $PM_{2.5}$ during the warm phase, possibly suggesting a bias in the material density calculation. This bias is likely due to the uncertainties in using chemical data from earlier studies (a

limitation of our work discussed in this paper) as well as the uncertainties associated with the method for the material density calculation. Nonetheless, the obtained shape factors, which were overall close to one, are in agreement with almost any study done in urban areas, indicating a nearly-spherical shape of ambient particles (Cross et al., 2007; Geller et al., 2006; Hu et al., 2012; Khlystov et al., 2004; McMurry et al., 1996). A more accurate estimation of shape factors admittedly requires parallel measurements of the apparent density and chemical composition of the sampled particles.

4. Summary and conclusions

The apparent densities of ambient fine and coarse particles were measured hourly during two separate seasons and their diurnal and seasonal variations were investigated. The apparent densities noticeably increased during the warmer phase, especially in the fine PM size fraction. This elevation for $PM_{2.5}$, during the summer, is mainly attributed to the decreased contribution of agglomerate soot particles, increased photochemical activity and production of secondary aerosols coupled with the condensation of these secondary materials on the pre-existing particles, filling out their void spaces. The enhanced contribution of resuspended road dust, enriched in metals and minerals, is mainly responsible for the increase in the CPM apparent density during the summer. Diurnal variation of $PM_{2.5}$ apparent density exhibited minima during the morning rush hours, in both phases. A similar drop was also observed during the afternoon rush hours of the cold phase. During mid-day, $PM_{2.5}$ apparent density increased to about 1.5 and 2.4 g cm^{-3} in the cold and warm phases, respectively. CPM apparent density in the cold phase displayed a minimum of about 1.4 g cm^{-3} during the morning traffic hours, then rapidly increased to about 1.8 g cm^{-3} and remained high until midnight. CPM apparent density during the warm phase exhibited minimum levels around 1.8 g cm^{-3}, from midnight until 7 a.m., to levels as high as 2.9 g cm^{-3} in early afternoon. The material density of particles was calculated from the chemical composition of fine and coarse PM, obtained from previous studies, and showed higher values during the summer in both size ranges. The dynamic shape factor of particles, calculated by the ratio of the material density to the apparent density, was generally close to 1 with slightly higher values during the winter.

Our findings provide important information on seasonal and diurnal variation of ambient fine and CPM apparent densities, which are direct result of complex and highly dynamic processes in an urban atmosphere that alter the chemical composition as well as the morphology of PM over different seasons, but also during the day.

Supplementary Material

Refer to Web version on PubMed Central for supplementary material.

Acknowledgments

References

Blando JD, Turpin BJ. Secondary organic aerosol formation in cloud and fog droplets: a literature evaluation of plausibility. Atmospheric Environment. 2000; 34:1623–1632.

Chen G, Ziemba LD, Chu DA, Thornhill KL, Schuster GL, Winstead EL, Diskin GS, Ferrare RA, Burton SP, Ismail S, Kooi SA, Omar AH, Slusher DL, Kleb MM, Reid JS, Twohy CH, Zhang H, Anderson BE. Observations of Saharan dust microphysical and optical properties from the Eastern Atlantic during NAMMA airborne field campaign. Atmos Chem Phys. 2011; 11:723–740.

Cheung K, Daher N, Kam W, Shafer MM, Ning Z, Schauer JJ, Sioutas C. Spatial and temporal variation of chemical composition and mass closure of ambient coarse particulate matter (PM10-2.5) in the Los Angeles area. Atmospheric Environment. 2011a; 45:2651–2662.

Cheung K, Daher N, Shafer MM, Ning Z, Schauer JJ, Sioutas C. Diurnal trends in coarse particulate matter composition in the Los Angeles Basin. Journal of environmental monitoring: JEM. 2011b; 13:3277–3287. [PubMed: 22025084]

Chou C, Stetzer O, Weingartner E, Jurányi Z, Kanji ZA, Lohmann U. Ice nuclei properties within a Saharan dust event at the Jungfraujoch in the Swiss Alps. Atmos Chem Phys. 2011; 11:4725–4738.

Clarke RW, Coull B, Reinisch U, Catalano P, Killingsworth CR, Koutrakis P, Kavouras I, Murthy GG, Lawrence J, Lovett E, Wolfson JM, Verrier RL, Godleski JJ. Inhaled concentrated ambient particles are associated with hematologic and bronchoalveolar lavage changes in canines. Environmental Health Perspectives. 2000; 108:1179–1187. [PubMed: 11133399]

Covert DS, Heintzenberg J, Hansson HC. Electro-optical Detection of External Mixtures in Aerosols. Aerosol Science and Technology. 1990; 12:446–456.

Cross ES, Slowik JG, Davidovits P, Allan JD, Worsnop DR, Jayne JT, Lewis DK, Canagaratna M, Onasch TB. Laboratory and Ambient Particle Density Determinations using Light Scattering in Conjunction with Aerosol Mass Spectrometry. Aerosol Science and Technology. 2007; 41:343–359.

DeCarlo PF, Slowik JG, Worsnop DR, Davidovits P, Jimenez JL. Particle Morphology and Density Characterization by Combined Mobility and Aerodynamic Diameter Measurements. Part 1: Theory. Aerosol Science and Technology. 2004; 38:1185–1205.

Delfino RJ, Sioutas C, Malik S. Potential Role of Ultrafine Particles in Associations between Airborne Particle Mass and Cardiovascular Health. Environmental Health Perspectives. 2005; 113:934–946. [PubMed: 16079061]

Delfino RJ, Staimer N, Tjoa T, Gillen DL, Polidori A, Arhami M, Kleinman MT, Vaziri ND, Longhurst J, Sioutas C. Air Pollution Exposures and Circulating Biomarkers of Effect in a Susceptible Population: Clues to Potential Causal Component mixtures and mechanisms. Environmental Health Perspectives. 2009; 117:1232–1238. [PubMed: 19672402]

Donaldson K, Stone V, Seaton A, MacNee W. Ambient particle inhalation and the cardiovascular system: potential mechanisms. Environmental Health Perspectives. 2001; 109:523–527. [PubMed: 11544157]

Ebert M, Weinbruch S, Hoffmann P, Ortner HM. The chemical composition and complex refractive index of rural and urban influenced aerosols determined by individual particle analysis. Atmospheric Environment. 2004; 38:6531–6545.

Fine PM, Chakrabarti B, Krudysz M, Schauer JJ, Sioutas C. Diurnal Variations of Individual Organic Compound Constituents of Ultrafine and Accumulation Mode Particulate Matter in the Los Angeles Basin. Environmental Science & Technology. 2004; 38:1296–1304. [PubMed: 15046329]

Geller M, Biswas S, Sioutas C. Determination of Particle Effective Density in Urban Environments with a Differential Mobility Analyzer and Aerosol Particle Mass Analyzer. Aerosol Science and Technology. 2006; 40:709–723.

Geller MD, Fine PM, Sioutas C. The Relationship between Real-Time and Time-Integrated Coarse (2.5–10 μm), Intermodal (1–2.5 μm), and Fine (<2.5 μm) Particulate Matter in the Los Angeles Basin. Journal of the Air & Waste Management Association. 2004; 54:1029–1039. [PubMed: 15468657]

Ghazi R, Olfert JS. Coating Mass Dependence of Soot Aggregate Restructuring due to Coatings of Oleic Acid and Dioctyl Sebacate. Aerosol Science and Technology. 2013; 47:192–200.

Hand JL, Kreidenweis SM. A New Method for Retrieving Particle Refractive Index and Effective Density from Aerosol Size Distribution Data. Aerosol Science and Technology. 2002; 36:1012–1026.

Hänel G. The real part of the mean complex refractive index and the mean density of samples of atmospheric aerosol particles. Tellus. 1968; 20:371–379.

Hasan H, Dzubay TG. Apportioning light extinction coefficients to chemical species in atmospheric aerosol. Atmospheric Environment (1967). 1983; 17:1573–1581.

Hering SV, McMurry PH. Optical counter response to monodisperse atmospheric aerosols. Atmospheric Environment. Part A. General Topics. 1991; 25:463–468.

Heyder J. Deposition of inhaled particles in the human respiratory tract and consequences for regional targeting in respiratory drug delivery. Proceedings of the American Thoracic Society. 2004; 1:315–320. [PubMed: 16113452]

Hinds, WC. Aerosol Technology: Properties, Behavior, and Measurement of Airborne Particles. John Wiley & Sons; 1999.

Hu M, Peng J, Sun K, Yue D, Guo S, Wiedensohler A, Wu Z. Estimation of Size-Resolved Ambient Particle Density Based on the Measurement of Aerosol Number, Mass, and Chemical Size Distributions in the Winter in Beijing. Environmental Science & Technology. 2012; 46:9941–9947. [PubMed: 22458861]

Hu S, Polidori A, Arhami M, Shafer MM, Schauer JJ, Cho A, Sioutas C. Redox activity and chemical speciation of size fractioned PM in the communities of the Los Angeles-Long Beach harbor. Atmos Chem Phys. 2008; 8:6439–6451.

Hussein T, Johansson C, Karlsson H, Hansson HC. Factors affecting non-tailpipe aerosol particle emissions from paved roads: On-road measurements in Stockholm, Sweden. Atmospheric Environment. 2008; 42:688–702.

Kaaden N, Massling A, Schladitz A, Müller T, Kandler K, Schütz L, Weinzierl B, Petzold A, Tesche M, Leinert S, Deutscher C, Ebert M, Weinbruch S, Wiedensohler A. State of mixing, shape factor, number size distribution, and hygroscopic growth of the Saharan anthropogenic and mineral dust aerosol at Tinfou, Morocco. Tellus B. 2009; 61:51–63.

Kent GS, Yue GK, Farrukh UO, Deepak A. Modeling atmospheric aerosol backscatter at CO2 laser wavelengths. 1: Aerosol properties, modeling techniques, and associated problems. Applied Optics. 1983; 22:1655–1665. [PubMed: 18196012]

Khalizov AF, Lin Y, Qiu C, Guo S, Collins D, Zhang R. Role of OH-Initiated Oxidation of Isoprene in Aging of Combustion Soot. Environmental Science & Technology. 2013; 47:2254–2263. [PubMed: 23379649]

Khlystov A, Stanier C, Pandis SN. An Algorithm for Combining Electrical Mobility and Aerodynamic Size Distributions Data when Measuring Ambient Aerosol Special Issue of Aerosol Science and Technology on Findings from the Fine Particulate Matter Supersites Program. Aerosol Science and Technology. 2004; 38:229–238.

Kostenidou E, Pathak RK, Pandis SN. An Algorithm for the Calculation of Secondary Organic Aerosol Density Combining AMS and SMPS Data. Aerosol Science and Technology. 2007; 41:1002–1010.

Li N, Sioutas C, Cho A, Schmitz D, Misra C, Sempf J, Wang MY, Oberley T, Froines J, Nel A. Ultrafine particulate pollutants induce oxidative stress and mitochondrial damage. Environmental Health Perspectives. 2003; 111:455–460. [PubMed: 12676598]

Majestic BJ, Schauer JJ, Shafer MM, Fine PM, Singh M, Sioutas C. Trace metal analysis of atmospheric particulate matter: A comparison of personal and ambient samplers The research described herein has not been subjected to the agency's required peer and policy review and therefore does not necessarily reflect the views of the agency, and no official endorsement should be inferred. Mention of trade names or commercial products does not constitute an endorsement or recommendation for use. Journal of Environmental Engineering and Science. 2008; 7:289–298.

Malloy QGJ, Nakao S, Qi L, Austin R, Stothers C, Hagino H, Cocker DR. Real- Time Aerosol Density Determination Utilizing a Modified Scanning Mobility Particle Sizer-Aerosol Particle Mass Analyzer System. Aerosol Science and Technology. 2009; 43:673–678.

McMurry PH, Wang X, Park K, Ehara K. The Relationship between Mass and Mobility for Atmospheric Particles: A New Technique for Measuring Particle Density. Aerosol Science and Technology. 2002; 36:227–238.

McMurry PH, Zhang X, Lee CT. Issues in aerosol measurement for optics assessments. Journal of Geophysical Research: Atmospheres. 1996; 101:19189–19197.

Misra C, Geller MD, Shah P, Sioutas C, Solomon PA. Development and Evaluation of a Continuous Coarse (PM10-PM25) Particle Monitor. Journal of the Air & Waste Management Association. 2001; 51:1309–1317. [PubMed: 11575884]

Moore KF, Ning Z, Ntziachristos L, Schauer JJ, Sioutas C. Daily variation in the properties of urban ultrafine aerosol--Part I: Physical characterization and volatility. Atmospheric Environment. 2007; 41:8633–8646.

Moore KF, Verma V, Minguillón MC, Sioutas C. Inter- and Intra-Community Variability in Continuous Coarse Particulate Matter (PM10-2.5) Concentrations in the Los Angeles Area. Aerosol Science and Technology. 2010; 44:526–540.

Nakao S, Shrivastava M, Nguyen A, Jung H, Cocker D. Interpretation of Secondary Organic Aerosol Formation from Diesel Exhaust Photooxidation in an Environmental Chamber. Aerosol Science and Technology. 2011; 45:964–972.

Ntziachristos L, Froines JR, Cho AK, Sioutas C. Relationship between redox activity and chemical speciation of size-fractionated particulate matter. Particle and Fibre Toxicology. 2007; 4

Ostro B, Lipsett M, Reynolds P, Goldberg D, Hertz A, Garcia C, Henderson KD, Bernstein L. Long-Term Exposure to Constituents of Fine Particulate Air Pollution and Mortality: Results from the California Teachers Study. Environmental Health Perspectives. 2009; 118:363–369. [PubMed: 20064787]

Pagels J, Khalizov AF, McMurry PH, Zhang RY. Processing of Soot by Controlled Sulphuric Acid and Water Condensation- Mass and Mobility Relationship. Aerosol Science and Technology. 2009; 43:629–640.

Pakbin P, Hudda N, Cheung KL, Moore KF, Sioutas C. Spatial and Temporal Variability of Coarse (PM10-2.5) Particulate Matter Concentrations in the Los Angeles Area. Aerosol Science and Technology. 2010; 44:514–525.

Pakbin P, Ning Z, Shafer MM, Schauer JJ, Sioutas C. Seasonal and Spatial Coarse Particle Elemental Concentrations in the Los Angeles Area. Aerosol Science and Technology. 2011; 45:949–963.

Park K, Cao F, Kittelson DB, McMurry PH. Relationship between particle mass and mobility for diesel exhaust particles. Environmental Science & Technology. 2003; 37:577–583. [PubMed: 12630475]

Park K, Kittelson DB, McMurry PH. Structural properties of diesel exhaust particles measured by transmission electron microscopy (TEM): Relationships to particle mass and mobility. Aerosol Science and Technology. 2004; 38:881–889.

Pitz M, Cyrys J, Karg E, Wiedensohler A, Wichmann HE, Heinrich J. Variability of Apparent Particle Density of an Urban Aerosol. Environmental Science & Technology. 2003; 37:4336–4342. [PubMed: 14572082]

Pitz M, Schmid O, Heinrich J, Birmili W, Maguhn, Zimmermann R, Wichmann HE, Peters A, Cyrys J. Seasonal and Diurnal Variation of PM2.5 Apparent Particle Density in Urban Air in Augsburg, Germany. Environmental Science & Technology. 2008; 42:5087–5093. [PubMed: 18754352]

Reid EA, Reid JS, Meier MM, Dunlap MR, Cliff SS, Broumas A, Perry K, Maring H. Characterization of African dust transported to Puerto Rico by individual particle and size segregated bulk analysis. Journal of Geophysical Research: Atmospheres. 2003; 108(D19):8591.

Reid JS, Cahill TA, Wakabayashi PH, Dunlap MR. Geometric/aerodynamic equivalent diameter ratios of ash aggregate aerosols collected in burning Kuwaiti well fields. Atmospheric Environment. 1994; 28:2227–2234.

Saffari A, Daher N, Shafer MM, schauer JJ, Sioutas C. Seasonal and spatial variation in dithiothretiol (DTT) activity of quasi-ultrafine particles in the Los Angeles Basin and its association with chemical species. Journal of Environmental Science and Health, Part A. 2013 In press.

Saldiva PHN, Clarke RW, Coull BA, Stearns RC, Lawrence J, Murthy GGK, Diaz E, Koutrakis P, Suh H, Tsuda A, Godleski JJ. Lung Inflammation Induced by Concentrated Ambient Air Particles Is Related to Particle Composition. American Journal of Respiratory and Critical Care Medicine. 2002; 165:1610–1617. [PubMed: 12070061]

Sardar SB, Fine PM, Sioutas C. Seasonal and spatial variability of the size-resolved chemical composition of particulate matter (PM10) in the Los Angeles Basin. Journal of Geophysical Research: Atmospheres (1984–2012). 2005; 110(D7)

Schulz H, Harder V, Ibald-Mulli A, Khandoga A, Koenig W, Krombach F, Radykewicz R, Stampfl A, Thorand B, Peters A. Cardiovascular Effects of Fine and Ultrafine Particles. Journal of Aerosol Medicine. 2005; 18:1–22. [PubMed: 15741770]

Schwarz JP, Spackman JR, Fahey DW, Gao RS, Lohmann U, Stier P, Watts LA, Thomson DS, Lack DA, Pfister L, Mahoney MJ, Baumgardner D, Wilson JC, Reeves JM. Coatings and their enhancement of black carbon light absorption in the tropical atmosphere. Journal of Geophysical Research: Atmospheres (1984–2012). 2008; 113(D3)

Shiraiwa M, Kondo Y, Moteki N, Takegawa N, Miyazaki Y, Blake DR. Evolution of mixing state of black carbon in polluted air from Tokyo. Geophysical Research Letters. 2007; 34:n/a–n/a.

Sioutas C, Abt E, Wolfson JM, Koutrakis P. Evaluation of the measurement performance of the scanning mobility particle sizer and aerodynamic particle sizer. Aerosol Science and Technology. 1999; 30:84–92.

Sioutas C, Kim S, Chang M, Terrell LL, Gong H Jr. Field evaluation of a modified DataRAM MIE scattering monitor for real-time PM2.5 mass concentration measurements. Atmospheric Environment. 2000; 34:4829–4838.

Stolzenburg M, Kreisberg N, Hering S. Atmospheric Size Distributions Measured by Differential Mobility Optical Particle Size Spectrometry. Aerosol Science and Technology. 1998; 29:402–418.

Strawa AW, Elleman R, Hallar AG, Covert D, Ricci K, Provencal R, Owano TW, Jonsson HH, Schmid B, Luu AP, Bokarius K, Andrews E. Comparison of in situ aerosol extinction and scattering coefficient measurements made during the Aerosol Intensive Operating Period. Journal of Geophysical Research: Atmospheres. 2006; 111:D05S03.10.1029/2005JD006056

Sun QWA. Long-term air pollution exposure and acceleration of atherosclerosis and vascular inflammation in an animal model. JAMA. 2005; 294:3003–3010. [PubMed: 16414948]

Turpin BJ, Huntzicker JJ, Larson SM, Cass GR. Los Angeles summer midday particulate carbon: primary and secondary aerosol. Environmental Science & Technology. 1991; 25:1788–1793.

Turpin BJ, Lim HJ. Species Contributions to PM2.5 Mass Concentrations: Revisiting Common Assumptions for Estimating Organic Mass. Aerosol Science and Technology. 2001; 35:602–610.

Wang D, Pakbin P, Shafer MM, Antkiewicz D, Schauer JJ, Sioutas C. Macrophage reactive oxygen species activity of water-soluble and water-insoluble fractions of ambient coarse, PM2.5 and ultrafine particulate matter (PM) in Los Angeles. Atmospheric Environment. 2013; 77:301–310.

Watson JG, Chow JC, Lowenthal DH, Stolzenburg MR, Kreisberg NM, Hering SV. Particle Size Relationships at the Fresno Supersite. Journal of the Air & Waste Management Association. 2002; 52:822–827. [PubMed: 12139347]

York D. Least-Squares Fitting of a Straight Line. Canadian Journal of Physics. 1966; 44:1079–1086.

- Hourly apparent density of ambient fine and coarse PM was measured in Los Angeles

- Apparent densities were higher during the warm season

- $PM_{2.5}$ apparent density showed minima during the traffic rush hours

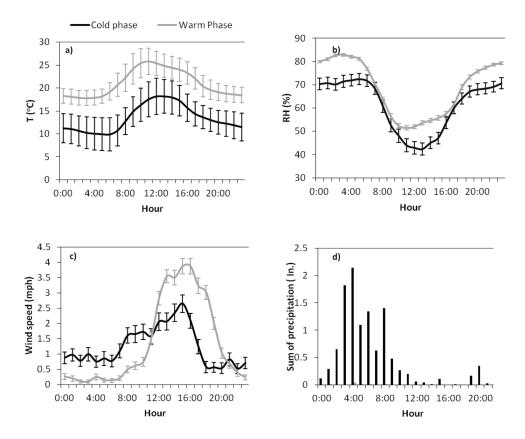- Coarse PM apparent density showed a similar diurnal trend with wind speed in summer

Figure 1.
a–d. Diurnal variations of: a) temperature, b) relative humidity, c) wind speed, and d) sum of precipitation, in the cold and warm phases. Error bars for temperature correspond to standard deviation and for relative humidity and wind speed correspond to one standard error.
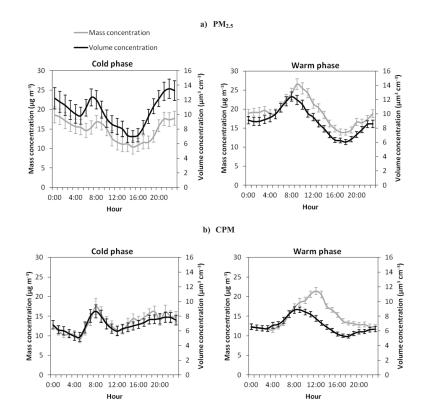
Figure 2.
a–b. Diurnal variations (geometric means) in the mass and volume concentrations of: a) PM$_{2.5}$ and b) CPM during the warm and cold phases. Error bars correspond to one standard error.
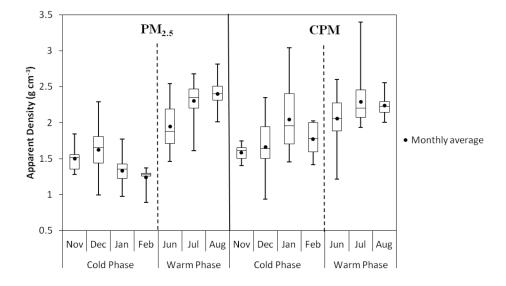
Figure 3.
Box plot of daily-averaged apparent density (g cm^{-3}) of PM$_{2.5}$ and CPM in each month during the cold and warm phases.
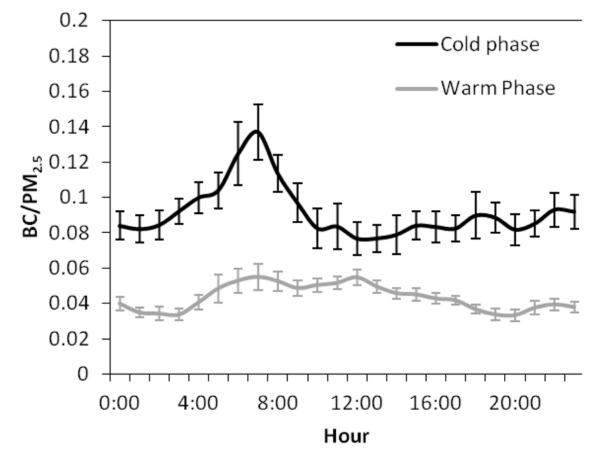
Figure 4.
Diurnal variation (geometric means) in the black carbon mass content of $PM_{2.5}$ ($BC/PM_{2.5}$) during the cold and warm phases. Error bars correspond to one standard error.
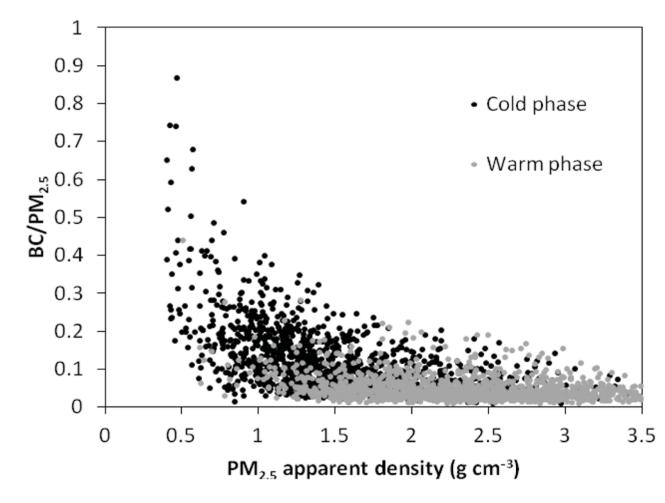
Figure 5.
Relationship between the hourly PM$_{2.5}$ apparent density (g cm^{-3}) and the black carbon mass content of PM$_{2.5}$ (BC/PM$_{2.5}$) in the cold and warm phases.
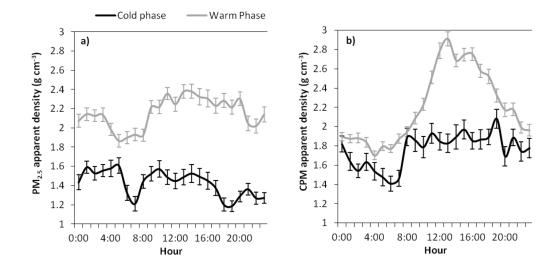
Figure 6.
a–b. Diurnal variations (geometric means) in the apparent density (g cm^{-3}) of: a) PM$_{2.5}$ and b) CPM during the cold and warm phases. Error bars correspond to one standard error.

Table 1

Spearman rank correlation coefficient between the hourly $PM_{2.5}$ and CPM apparent densities and other parameters during the cold and warm phases.

	T^a	RH^b	$BC/PM_{2.5}$
Cold Phase			
$PM_{2.5}$ apparent density	0.10	0.09	−0.56
CPM apparent density	0.14	−0.39	-
Warm Phase			
$PM_{2.5}$ apparent density	0.23	−0.12	−0.25
CPM apparent density	0.42	−0.41	-

[a] Temperature,

[b] Relative humidity

Note: All correlations were statistically significant at 0.05 level

Table 2

Material and apparent densities (g cm^{-3}) and dynamic shape factors (DSF) (±standard deviation) of PM$_{2.5}$ and CPM during the summer and winter.

	Summer	Winter
Material density (g cm^{-3})		
Cheung et al., 2011a **(CPM)**	2.28 ± 0.03	2.00 ± 0.09
Cheung et al., 2011b **(CPM)**	2.44 ± 0.05	2.13 ± 0.03
Sardar et al., 2005 **(PM$_{2.5}$)**	1.71 ± 0.30	1.41 ± 0.44
Apparent density (g cm^{-3})		
Current study (CPM)	2.21 ± 0.38	1.76 ± 0.18
Current study (PM$_{2.5}$)	2.16 ± 0.16	1.43 ± 0.13
DSF		
CPM	1.07 ± 0.18	1.17 ± 0.13
PM$_{2.5}$	0.79 ± 0.15	0.99 ± 0.32